ISSN 1674-1056
http://cpb.iphy.ac.cn
http://iopscience.iop.org/cpb
中国物理 B
Chinese Physics
中国物理 Chinese Physics B

Directional mechanical and thermal properties of single-layer black phosphorus by classical molecular dynamics

Afira Maryam, Ghulam Abbas, Muhammad Rashid, Atif Sattar
Citation: Chin. Phys. B . 2018, 27(1): 017401. **doi:** 10.1088/1674-1056/27/1/017401

Journal homepage: http://cpb.iphy.ac.cn; http://iopscience.iop.org/cpb

What follows is a list of articles you may be interested in

Electromechanical actuation of CNT/PVDF composite films based on a bridge configuration

Xiaogang Gu(谷孝刚), Xiaogang Xia(夏小刚), Nan Zhang(张楠), Zhuojian Xiao(肖卓建), Qingxia Fan(范庆霞), Feng Yang(杨丰), Shiqi Xiao(肖仕奇), Huiliang Chen(陈辉亮), Weiya Zhou(周维亚), Sishen Xie(解思深)
Chin. Phys. B . 2017, 26(7): 078101. **doi:** 10.1088/1674-1056/26/7/078101

Carbon-nanodot-coverage-dependent photocatalytic performance of carbon nanodot/TiO_2nanocomposites under visible light

Ming-Ye Sun(孙明烨), You-Jin Zheng(郑友进), Lei Zhang(张蕾), Li-Ping Zhao(赵立萍), Bing Zhang(张冰)
Chin. Phys. B . 2017, 26(5): 058101. **doi:** 10.1088/1674-1056/26/5/058101

Multiband nodeless superconductivity near the charge-density-wave quantum critical point in $ZrTe_{3-x}Se_x$

Shan Cui(崔珊), Lan-Po He(何兰坡), Xiao-Chen Hong(洪晓晨), Xiang-De Zhu(朱相德), Cedomir Petrovic, Shi-Yan Li(李世燕)
Chin. Phys. B . 2016, 25(7): 077403. **doi:** 10.1088/1674-1056/25/7/077403

Effect of residual stress on nematic domains in $BaFe_{2-x}Ni_xAs_2$ studied by angular magnetoresistance

Ding Hu(胡定), Wenliang Zhang(张汶良), Yuan Wei(魏源), Xiaotian Zhang(张笑天), Cong Ren(任聪), Lei Shan(单磊), Yi-feng Yang(杨义峰), Huiqian Luo(罗会仟), Shiliang Li(李世亮)
Chin. Phys. B . 2016, 25(5): 057402. **doi:** 10.1088/1674-1056/25/5/057402

Thermal and thermoelectric response from Keldysh formalism with application to gapped Dirac fermions

Zhu Guo-Bao, Yang Hui-Min, Yang Sheng-Yuan
Chin. Phys. B . 2015, 24(4): 047401. **doi:** 10.1088/1674-1056/24/4/047401

Directional mechanical and thermal properties of single-layer black phosphorus by classical molecular dynamics

Afira Maryam[1], Ghulam Abbas[2], Muhammad Rashid[3,†], and Atif Sattar[4]

[1] *Department of Physics, Riphah International University, Islamabad, Pakistan*
[2] *Department of Nanoscience and Nanotechnology, Research Institute of Physics and Chemistry, Chonbuk National University, Jeonju, Chonbuk* 561-756, *Republic of Korea*
[3] *Department of Physics, COMSATS Institute of Information Technology, Islamabad* 44000, *Pakistan*
[4] *Department of Physics Simulation Laboratory, The Islamia University of Bahawalpur*, 63100, *Pakistan*

(Received 22 August 2017; revised manuscript received 30 September 2017; published online 28 November 2017)

Black phosphorus (BP) has received attention due to its own higher carrier mobility and layer dependent electronic properties, such as direct band gap. Interestingly, the single layer black phosphorus (SLBP) has had large popularity in applications related to thermoelectric, optoelectronic, and electronic devices. Here, we investigate the phonon spectrum, thermal conductivities, and stress strain effects. Robust anisotropy was mainly observed in the thermal conductivities together with the alongside zigzag (ZZ) direction value, compared to the armchair (AC) directions. We also investigated the attitude of stress that was anisotropic in both directions, and the stress effects were two times greater across the ZZ path than those in the AC direction at a low temperature. We obtained a Young's modulus of 63.77 and 20.74 GPa in the AC and ZZ directions, respectively, for a strain range of 0.01. These results had good agreement with first principle calculations. Our study here is useful and significant for the thermal tuning of phosphorus-based nanoelectronics and thermalelectric applications of phosphorus.

Keywords: electric and thermal conductivity, molecular dynamics methods, carbon/carbon-based materials

PACS: 74.25.fc, 47.11.Mn, 81.05.U– **DOI:** 10.1088/1674-1056/27/1/017401

1. Introduction

In recent years, two-dimensional (2D) materials have played a vital role due to their unique and flexible properties. The electronics, optical, thermal, and mechanical properties show interesting features useful in industry, as well as for research purposes.[1–3] From an application point of view, these low dimension layer materials have received a great deal of attention and are attractive for use in electronic and optical devices.[4–7] They are not only limited to these applications, but have also been considered as candidates for future energy efficient devices.[8] Numerous supplementary types of 2D materials, for example transition metal di-chalcogenides (TMDs), black phosphorus (BP), and transition metal oxides (TMOs), have also received a great deal of attention.[9] This is due to scientists, engineers, and researchers that have explored the interesting results with accuracy and perfection. After the discovery of graphene,[10] great research interest has grown in the scientific community involved in this emerging field and the low dimension characterictics of different materials have been explored. After very skillful and meaningful considerations involving a great deal of effort, many other materials have been fabricated, such as phosphorene,[11] silicine,[12–14] and TMDs.[15–17] Previously, high electronic mobility had been established in few-layer BPs and which were practical and useful in field-effect transistors (FET).[18] BPs is an emerging material, having characteristics related to optical, electrical, and thermal properties, having more interesting benefits for applications in the field of optoelectronics and photonics devices.

In the periodic table, the phosphorous element is at No. 15 in the group 5A. BP, that is probably the most stable structural framework on the list of phosphorus allotropes, is used in semiconductor materials produced together with sp^3-hybridized bonds. In recent years, single layer of black phosphorous (SLBP), like brand new 2D materials, has gained interest because of its distinctive electronic properties, such as more than 10^4 drain current modulation, adjustable direct gap, and higher charge-carrier range of motion (as much as 10^3 $cm^2 \cdot V \cdot s$). 2D materials like silicence, graphene, and MoS_2 have been studied intensively because of the abundant physics and the prospect of direct integration into next-generation electronics and energy conversion process gadgets. Instead of their own bulk counterparts, the optical, electronic, vibrational, mechanical, and thermal properties, could be very easily personalized via the use of exterior strain, as well as exposing flaws and bunching several levels from the reduced dimensional supplies. As an example, the thermal conductivity associated with readily hanging solitary coating graphene decreased from 3000–5000 to 600 $W \cdot m^{-1} \cdot K^{-1}$ by placing into amorphous SiO_2.[19] This preliminary enthusiasm surrounding BP is distinct as in the case of graphene. BP has a direct bandgap that is layer dependent.[20]

†Corresponding author. E-mail: rapakistanaa@gmail.com

© 2018 Chinese Physical Society and IOP Publishing Ltd

Currently, BP is produced by scaling a few layers from bulk BP.[21,22] BP includes a honeycomb framework much like graphene, however it is actually non-planar. BP has a direct band gap of 2 eV.[23] The band gap can be increased by reducing the number of levels and decreased by increasing layers, so that it has 0.3 eV in the bulk phase. The overall performance features, that are comparable or even better than additional 2D materials, can be accomplished for any bulk phosphorus dependent transistor.[24] Through additional 2D supplies, the BP anisotropic framework can lead to reliant optical, mechanized, thermal, and electronic properties modified by up to 50%.[25]

The focus is to research the lattice thermal conductivity associated with SLBP. Ong *et al.* looked into results associated with stress for the ballistic thermal conductance of BP utilizing non-equilibrium Green's functions depending on harmonic lattice dynamics. In this theoretical research work, molecular dynamics (MD) simulations were performed using the Stillinger–Weber (SW) potential to study the structural properties and thermal conductivities of SLBP within the diffusive transportation routine by describing phonon-phonon scattering. The results associated with mechanical strain regarding the thermal conductivity of SLBP are investigated.

2. Computational details

The SW potential is a sum of a couple of physique phrases and a three body terms potential. It was introduced in 1985 and gained significant popularity. The SW potential is one of the best potentials to be used for a diamond lattice (e.g., Si, GaAs, Ge, and C).[26] The description of bonding in SLBP requires a prediction that every atom offers six neighbors a hexagonal structure because of the most relaxed atomic arrangement. Directional bonding is introduced in a SW potential through explicit three body terms of the potential energy expansion. In addition, three body terms correct the intra and inter group angles. The SW potential can be written as

$$U(r_1, r_2, \ldots, r_n) = \sum_{ij} U_2(r_i, r_j) + \sum_{i,j,k} \sum_{i<j<k} U_3(r_i, r_j, r_k).$$

The first term and second terms represent the two and three body parts of the SW potential,

$$U_2(r) = A\varepsilon\{B\left(\frac{\sigma}{r}\right)^p - \left(\frac{\sigma}{r}\right)^q \times \exp\left(\frac{\sigma}{r-a\sigma}\right),$$

$$U_3(r,s,\vartheta) = \lambda\varepsilon(\cos\vartheta - \cos\vartheta o)^2 \exp\left(\frac{\sigma\gamma}{r-a\sigma}\right) \times \exp\left(\frac{\sigma\gamma}{r-a\sigma}\right).$$

The SW potential two body terms are functions of the distance between the pairs of atoms, and the three body terms depend upon the distance and triplet angle formed between the pairs of atoms. The angular part of the SW potential is due to the different values of the triplet angles, which form between pairs of atoms and are produced by bond bending or stretching. The interaction parameter λ scales to the strength of interactions and tunes the geometry of the SLBP model. The energy scale parameter (ε) tunes the energy and depth of the two-body interaction, and the length (σ) scale parameter sets the diameter of the particles.[27]

We can write the SW potential in a reduced form with the independence of the ε and σ parameters. The parameters A, B, p, q, and γ scale the potential expression and the reduced cutoff parameter ensures that all forces and energy at ($a = a\sigma$) become zero. We executed molecular dynamics (MD) simulations by using LAMMPS MD software that was produced by Sandia National Labs. The thermal conductivity was obtained by using the Green–Kubo equilibrium formalism by applying classical molecular dynamics. Typically, the periodic boundary factors were used in all directions. A time of 10 ps was used to relax the structure at a zero pressure. We used a 10 ns MD simulation time to calculate the properties of the SLBP. Therefore, the temperature and pressure was managed using the Nose–Hoover thermostat and barostat, respectively.

After thermalization, the structure of the SLBP extended in a single path at a strain rate of 10^8 s^{-1} and stress within the horizontal direction was permitted to finally achieve complete relaxation. The system included 5832 contaminants inside a regular container. The phonon spectrum and density of states were computed using a unit cell of SLBP. Table 1 provides the SW potential parameters that were used by LAMMPS.

Table 1. The LAMMPS parameter of the Stillinger–Weber potential for the SLBP.

	ε[a]/eV	σ[b]/Å	a	λ[c]	γ	cos θ	A	B	p	q	Tol
P_a–P_a–P_a	1.000	0.809	3.449	35.701	1.000	–0.111	3.626	33.371	4.0	0.0	0.0
P_b–P_b–P_b	1.000	0.809	3.449	35.701	1.000	–0.111	3.626	33.371	4.0	0.0	0.0
P_a-P_a–P_a	1.000	0.809	3.449	32.001	1.000	–0.210	0.000	33.371	4.0	0.0	0.0
P_b–P_b–P_b	1.000	0.809	3.4449	32.001	1.000	–0.210	0.000	33.371	4.0	0.0	0.0

[a]The energy scale parameter to control the depth of the two body interaction term.
[b]The length scale parameter to tune the diameter of the particles in the model.
[c]The repulsive three body interaction term to determine the strength of the interaction in the model.

3. Results and discussions

Black phosphorus is the most stable allotrope of all carbon materials. The layered construction is comprised of sheets of phosphorus atoms organized inside a puckered honeycomb unit cell. Adjoining cellular layers interact by means of van der Waals forces and therefore are inside a stacking arrangement.

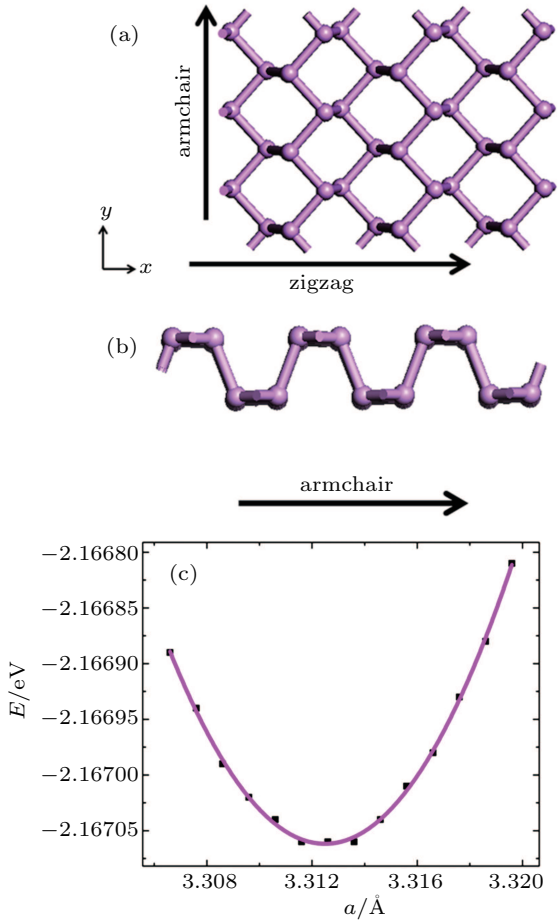


Fig. 1. (color online) Chemical structure of SLBP. The (a) ZZ and (b) AC directions are along the x and y directions, respectively. (c) Structural optimization plot of SLBP.

In addition, the in-plane bonds are stronger in the SLBP structure. On the other hand, the van der Waals inter-layer interactions are weaker. Figures 1(a) and 1(b) show a representation of the single layer black phosphorus chemical structure in Zigzag (ZZ) and armchair (AC) directions in the x–y plane. The structural properties are very important to understand the material properties at the microscopic level. We have characterized the structure stability through lattice optimization. The energy was a function of the lattice constant energy, that changes when the lattice constant was varied. We obtained an optimized lattice constant for which the energy became a minimum, as shown in Fig. 1(c). The exact minimum value of the energy was found by the least square $f(x) = ax + bx^2 + c$ fit equation. The angle distribution function

$$D(\theta) = \frac{1}{Nn_\theta} \sum_{k=1}^{N} \sum_{i=1}^{n_c} \sum_{j\neq i}^{n_c-1} \delta(\theta - \theta_{ikj})$$

was computed as an ensemble average over the angles between each of the SLBP pairs of phosphorus atoms and its closest n_c neighbours n_θ represents the number of angles subtended by the nearest neighbours (n_c) of the central atom around θ_{ikj}. The bond distribution function

$$D(r) = \frac{1}{N} \sum_{k=1}^{N} \sum_{i=1}^{n_c} \sum_{j\neq i}^{n_c-1} \delta(r - r_{ikj})$$

was computed as an ensemble average over the distance between each pair of phosphorus atoms and its closest n_c neighbours. r_{ikj} represents the distance of an atom close to the nearest neighbours (n_c) of the central atom. On the other hand, Figures 2(a) and 2(b) show bond-length and bond-angle distribution functions, respectively, of the relaxed single layer black phosphorus atom structure, obtained using the SW potential. The maximum bond-length was 2.5 Å and maximum bond-angle was 97.97° throughout the symmetry of a relaxed atom structure of the SLBP.

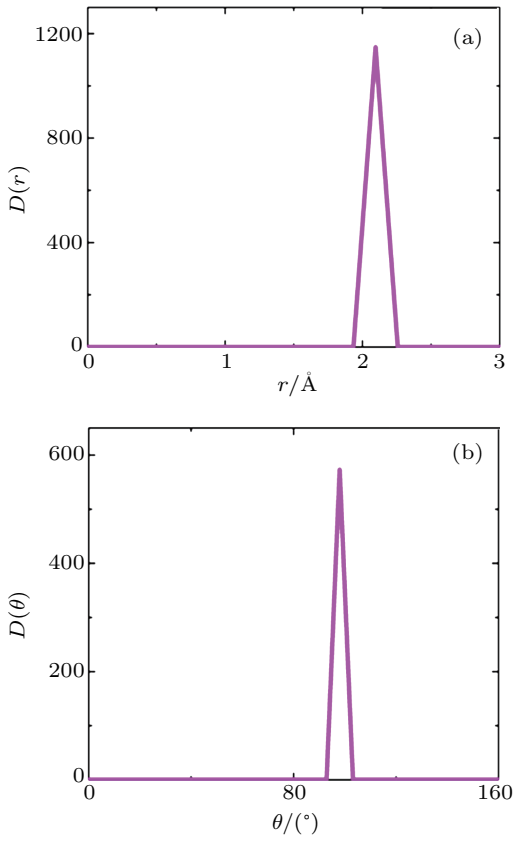


Fig. 2. (color online) (a) Bond-length distribution $D(r)$ and (b) bond-angle distribution $D(\theta)$ of the relaxed SLBP at zero pressure using the Stillinger–Weber potential.

For SLBP, figures 3(a) and 3(b) indicate the phonon dispersion contour across the higher symmetry directions of the

Brillion Zone and the normalized phonon density of states, respectively. The phonon dispersion curve closely matched those reported by Jiang.[28,29] The unit cell of the SLBP has four atoms, leading to a dozen dispersal divisions. The upmost phonon frequency in this allotrope was 330 cm^{-1}, but the band gap was (0.01 eV = 111 cm^{-1}) in the SLBP due to the symmetry of the crystal and numerous modalities along the particular route at exactly the same frequency.[29] At the gamma point, there were exactly three modes, that linearly decreased and their frequencies became zero. These were six acoustic modes, so the high frequency three modes were longitudinal acoustic modes and lower frequency modes were transverse. The other six modes, with higher frequencies, were optical modes. In the normalized phonon density of states, we observed the band gap between the acoustic and optical modes in the same range as in the phonon dispersion spectrum. The frequency of the optical modes was higher compared with the acoustic modes.

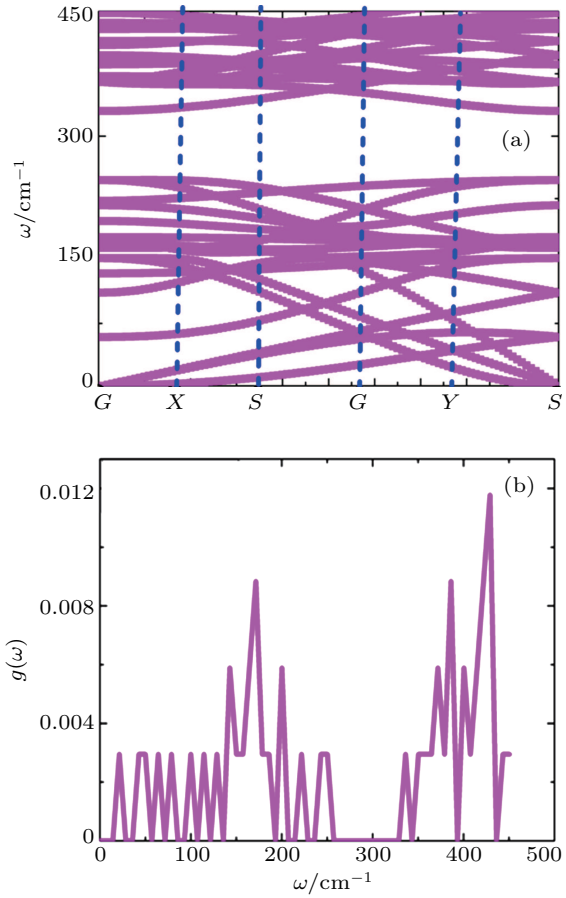


Fig. 3. (color online) Phonon dispersion curve (a) and normalized phonon density of states (b) of an SLBP.

Figure 4(a) displays the thermal conductivity (κ) of the SLBP at different temperatures from 200 to 500 K. It was observed that the thermal conductivity (κ) of the SLBP is anisotropic within each AC as well as the ZZ directions. We predicted the layer thickness for the thermal conductivity (κ) calculation and choose 5.25 Å bulk separations for the SLBP. The thermal conductivity (κ) was reduced with increasing temperature, which was not surprising for any phonon centred inside a crystalline material. At an ambient condition (300 K), the anticipated thermal conductivities (κ) were 110 and 36 $W{\cdot}m^{-1}{\cdot}K^{-1}$ in the ZZ and AC directions, respectively.[17] The thermal conductivity (κ) within the ZZ path was three times greater than that within the AC path. This anisotropy may be helpful within the layout, regarding temperature channelling inside micro and nano devices. We attributed the anisotropy due to the thermal conductivity (κ) because of the anisotropic phonon dispersal.

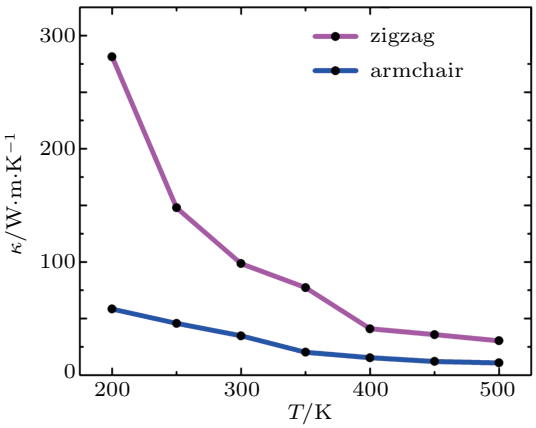


Fig. 4. (color online) Thermal conductivity of SLBP is in the ZZ and AC directions.

Figure 4 shows that the thermal conductivities (κ) across the ZZ and AC paths are 99 and 34 $W{\cdot}m^{-1}{\cdot}K^{-1}$, respectively, comparable to those obtained by Ankit and Alan (110 W and 36 $W{\cdot}m^{-1}{\cdot}K^{-1}$). The thermal conductivity (κ) of the SLBP inside the ZZ course can be compared with the value for the MoS_2 sample of 10 μm for ambient conditions (108 $W{\cdot}m^{-1}{\cdot}K^{-1}$) obtained by Lindsay *et al.*[22] The predicted thermal conductivity (κ) associated with graphite is 3600 $W{\cdot}m^{-1}{\cdot}K^{-1}$, thirty times greater than the thermal conductivity (κ) of the SLBP. The reduced thermal conductivity (κ) of the SLBP was a result of the scaled-down sound velocities (40000–8000 ms^{-1} in comparison to 21300 ms^{-1} in graphene), lower Debye temperature (500 K compared to 21300 K for graphene), more phonon scattering rates at room temperature, and because of plane symmetry.[13–18] The out-plane symmetry existence in a graphene structure limits the involvement of an odd number of the ZA funnies' in phonon-phonon scattering events. The predicted factor associated with the ZA phonons for the thermal conductivity (κ) within the black phosphorus differed by 12%–44% compared with 76% for graphite at ambient conditions.[17] The thermal conductivity (κ) factors for the various traditional acoustic phonon divisions within the SLBP acted like individual predictions of MoS_2.[22] Additionally, it offered a non-planar framework. Moreover, for the freely suspended single

layer graphene deposited on amorphous SiO_2 at room temperature, the thermal conductivity (κ) was reduced from 5000 to 600 $W{\cdot}m^{-1}{\cdot}K^{-1}$ [24] due to the increase in the scattering of ZA phonons. However, the thermal conductivity (κ) of single layer graphene experienced a decrease compared with the increase of a factor of five. In an SLBP, the contribution of the ZA phonons is 31% and 12% along the ZZ and AC directions, respectively. We assumed an equivalent reduction in the thermal conductivity (κ) of the reinforced SLBP sample calculated with the SW potential.

Figure 5 shows the stress strain curve of the SLBP subjected to tensile deformation along the ZZ and AC directions. The periodic boundary ailments utilized inside the equal guidelines. The system was thermalized to the equilibrium condition with NPT (constant number of particles, pressure, and temperature) ensembles for 1 ns by the Nose-Hover approach. After equilibrium, the structure of SLBP extended in a single path from a strain rate of 10^7 s^{-1} as well as stress within the horizontal path permitted to reach complete relaxation. The inter layer was fixed at a distance of 5.24 Å as a thickness of the SLBP in the calculation of the strain energy density. We obtained a Young modulus of 63.77 and 20.74 GPa in the AC and ZZ paths, respectively, in the strain range of 0.01. These values agreed well with those reported by Qiao, of 28.9 and 101.1 $N{\cdot}m^{-1}$ along the AC and ZZ directions, respectively.[16] Figure 5 shows that the SLBP produced less strain at room temperature (300 K), compared with the low temperature (1.0 K) along with the AC and ZZ paths. The stress was anisotropic in both directions, but the stress was two times greater in the ZZ direction compared with the AC direction at low temperature, implying that the attitude of the stress was anisotropic along these directions.

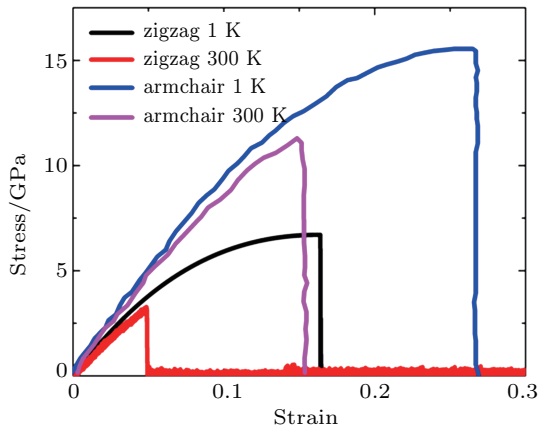


Fig. 5. (color online) Stress-strain curve of the SLBP at room temperature 300 K and 1 K in the ZZ and AC directions.

Neglecting local field effects, the imaginary part of the frequency-dependent dielectric matrix is determined by

$$\varepsilon^2_{\alpha\beta}(\omega) = \frac{4\pi^2 e^2}{\Omega} \lim_{q\to 0} \frac{1}{q^2} \sum_{c,v,\boldsymbol{k}} 2w_k \delta(\varepsilon_{c\boldsymbol{k}} - \varepsilon_{v\boldsymbol{k}} - \omega) \times \langle u_{c\boldsymbol{k}+\boldsymbol{e}_\alpha q} | u_{v\boldsymbol{k}} \rangle \langle u_{c\boldsymbol{k}+\boldsymbol{e}_\beta q} | u_{v\boldsymbol{k}} \rangle^*,$$

where the indices c and v refer to the conduction and valence band states, respectively; $w_{\boldsymbol{k}}$ is the weight of the $\boldsymbol{k}$-point; and $u_{c\boldsymbol{k}}$ is the cell periodic part of the orbitals at the $\boldsymbol{k}$-point. The real part of the tensor $\varepsilon^1_{\alpha\beta}(\omega)$ was obtained from the Kramers–Kronig relation. The absorption $\alpha(\omega)$ and extinction $\kappa(\omega)$ coefficients are determined from ε_1 and ε_2 using

$$\alpha(\omega) = \frac{2\omega}{c}\sqrt{\frac{|\varepsilon(\omega)| + \varepsilon_1(\omega)}{2}}, \quad |\varepsilon(\omega)| = \sqrt{\varepsilon_1^2 + \varepsilon_2^2},$$
$$\kappa(\omega) = \frac{2\omega}{c}\sqrt{\frac{|\varepsilon(\omega)| - \varepsilon_1(\omega)}{2}},$$

Figure 6 shows the extinction $\kappa(\omega)$ and absorption $\alpha(\omega)$ coefficients of a single layer BP. It shows much higher absorption and extinction coefficients in the UV light regions (200–390 nm). It clearly shows that the single layer black and blue phosphorus were able to harvest the UV light more efficiently.[30] Therefore, the single layer black phosphorus is useful for potential applications in efficient solar cells and ultrathin optoelectronic devices.

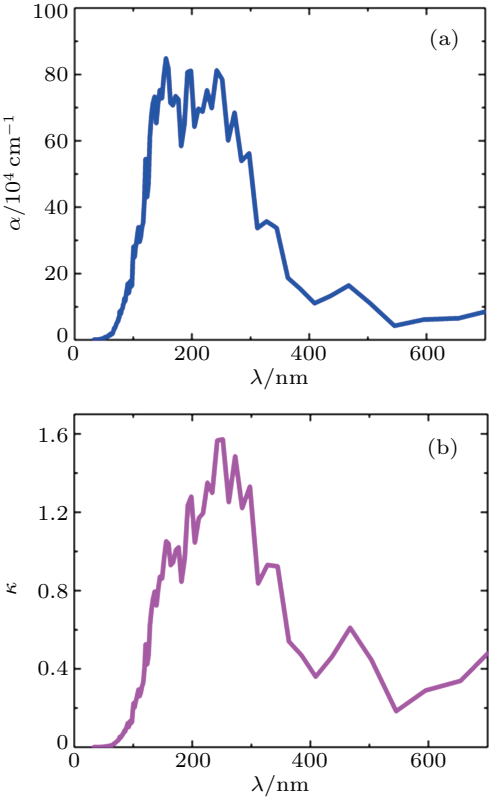


Fig. 6. (color online) (a) Absorption coefficient $\alpha(\omega)$ and (b) extinction coefficient $\kappa(\omega)$ of single layer black phosphorus.

4. Conclusion

By using the SW potential, we examined phonon dispersion and thermal conductivity at different temperatures of the SLBP and observed stress strain effects at room and low temperatures. We observed a decrease in the thermal conductivity with increasing temperature and at room temperature (300 K)

the thermal conductivities were 110 and 36 $W \cdot m^{-1} \cdot K^{-1}$ along the ZZ and AC paths, respectively. We were able to determine which thermal conductivity within the ZZ path was 3 times greater than that in the AC direction. We obtained a Young modulus of 63.77 and 20.74 in the AC and ZZ directions, respectively, that agreed with first principle calculations. The maximum phonon frequency in this allotrope was 330 cm^{-1} and the phonon band gap was 0.01 eV in the SLBP. These findings suggest a technique to model the thermal properties of the SLBP for prospective applications in heat channeling for micro and nano-devices, such as transistors and batteries.

References

[1] Akhtar M, Anderson G, Zhao R, Alruqi A, Mroczkowska J E, Sumanasekera G and Jasinski J B 2017 *npj 2D Mater. Appl.* **1** 5
[2] Aufray B, Kara A, Vizzini S, Oughaddou H, Léandri C, Ealet B and Le Lay G 2010 *Appl. Phys. Lett.* **96** 183102
[3] Efetov D K and Kim P 2010 *Phys. Rev. Lett.* **105** 256805
[4] Hu T, Han Y and Dong J 2014 *Nanotechnology* **25** 455703
[5] Jiang J W 2015 *Nanotechnology* **26** 315706
[6] Jiang J W and Park H S 2014 *Nat. Commun.* **5** 1
[7] Li C and Broido D 2017 *Phys. Rev. B* **95** 205203
[8] Li L, Yu Y, Ye G J, Ge Q, Ou X, Wu H, Feng D, Chen X H and Zhang Y B 2014 *Nat. Nanotechnol.* **9** 372
[9] Guo Z, Zhang H, Lu S, Wang Z, Tang S, Shao J, Sun Z, Xie H, Wang H, Yu X and Chu P K 2015 *Adv. Funct. Mater.* **25** 6996
[10] Li S and Chen Y 2017 *Sci. Rep.* **7** 43956
[11] Li W, Yang Y, Zhang G and Zhang Y W 2015 *Nano Lett.* **15** 1691
[12] Li W, Carrete J and Mingo N 2013 *Appl. Phys. Lett.* **103** 253103
[13] Liu B, Meng F, Reddy C D, Baimova J A, Srikanth N, Dmitriev S V and Zhou K 2015 *RSC Adv.* **5** 29193
[14] Mickevičius R and Zhao J H 1998 *J. Appl. Phys.* **83** 3161
[15] Mohr M, Maultzsch J, Dobardžić E, Reich S, Milošević I, Damnjanović M, Bosak A, Krisch M and Thomsen C 2007 *Phys. Rev. B* **76** 035439
[16] Molinero V and Moore E B 2008 *J. Phys. Chem. B* **113** 4008
[17] Qiao J, Kong X, Hu Z X, Yang F and Ji W 2014 *Nat. Commun.* **5** 1
[18] Lu S B, Miao L L, Guo Z N, Qi X, Zhao C J, Zhang H, Wen S C, Tang D Yand Fan D Y 2015 *Opt. Express* **23** 11184
[19] Rodin A, Carvalho A and Neto A C 2014 *Phys. Rev. Lett.* **112** 176801
[20] Jiang J W 2015 *Nanotechnology* **26** 055701
[21] Sa B, Li Y L, Sun Z, Qi J, Wen C and Wu B 2015 *Nanotechnology* **26** 215205
[22] Seol J H, Jo I, Moore A L, Lindsay L, Aitken Z H, Pettes M T, Li X, Yao Z, Huang R, Broido D and Mingo N 2010 *T Science* **328** 213
[23] Wang H, Liu Y, Li M, Huang H, Xu H M, Hong R J and Shen H 2010 *Optoelectron. Adv. Mater. Rapid. Commun.* **4** 1166
[24] Xia F, Wang H and Jia Y 2014 *Nat. Commun.* **5** 4458
[25] Liu H, Neal A T, Zhu Z, Luo Z, Xu X, Tománek D and Ye P D 2014 *ACS Nano* **8** 4033
[26] Zhang T, Lin J H, Yu Y M, Chen X R and Liu W M 2015 arXiv: 1502.01805
[27] Zhang Y, Pei Q and Wang C 2012 *Appl. Phys. Lett.* **101** 081909
[28] Zhang Y Y, Pei Q X, Jiang J W, Wei N and Zhang Y W 2016 *Nanoscale* **8** 483
[29] Sa B, Li Y L, Qi J, Ahuja R and Sun Z 2014 *J. Phys. Chem. C* **118** 26560
[30] Peng Q, Wang Z, Sa B, Wu B and Sun Z 2016 *Sci. Rep.* **6** 31994